Electronic structure of Cu_3N films studied by soft x-ray spectroscopy

2008 J. Phys.: Condens. Matter 20 235212

(http://iopscience.iop.org/0953-8984/20/23/235212)

J. Phys.: Condens. Matter **20** (2008) 235212 (7pp) doi:10.1088/0953-8984/20/23/235212

Electronic structure of Cu_3N films studied by soft x-ray spectroscopy

A Modin[1], K O Kvashnina[1], S M Butorin[1], L Werme[1], J Nordgren[1], S Arapan[1,2], R Ahuja[1,3], A Fallberg[4] and M Ottosson[4]

[1] Department of Physics, Uppsala University, PO Box 530, SE-751 21 Uppsala, Sweden
[2] Institute of Electronic Engineering and Industrial Technologies, Academy of Sciences of Moldova, Academiei 3/3, MD-2028 Chisinau, Moldova
[3] Applied Materials Physics, Department of Materials and Engineering, Royal Institute of Technology (KTH), S-100 44 Stockholm, Sweden
[4] Department of Materials Chemistry, Uppsala University, PO Box 538, SE-751 21 Uppsala, Sweden

Received 28 December 2007, in final form 8 April 2008
Published 6 May 2008
Online at stacks.iop.org/JPhysCM/20/235212

Abstract
Soft x-ray emission spectroscopy was used to characterize the electronic structure of seven copper nitride films, one synthesized with atomic layer deposition (ALD) and six grown with chemical vapor deposition (CVD) at different preparation temperatures. Interpretation of the x-ray emission spectra was supported by calculations of the electronic structure for bulk pure Cu_3N and Cu_3N with: an excess of Cu atoms, oxygen or carbon impurities, and N vacancies. The calculations are shown to describe the experimental spectra quite well. Analysis of the x-ray spectra suggests that films grown in copper rich environments and above a cut-off temperature of approximately 360 °C have a growing fraction of copper enriched areas, while films prepared below this temperature do not have these areas with excess copper.

1. Introduction

Semiconductor devices have been studied for over 130 years [1]. Ever since the discovery of the transistor [2, 3], these materials have attracted the interest of scientists in fundamental research as well as in industrial laboratories around the world. The main reason for this great interest is that semiconductor devices are the foundation of the electronic industry, which today is the largest industry in the world.

Copper nitride (Cu_3N) is a semiconductor where the bandgap varies with the nitrogen content. In copper rich environments Cu_3N films can obtain a metallic character with bandgaps as low as 0.25 eV for films with low resistivity and larger unit cells [4, 5]. For Cu_3N films with an insulating character, bandgaps in the range of 1.1–1.8 eV have been reported [5–10]. Cu_3N has a cubic anti-ReO_3 structure and in copper rich environments it has been proposed that an extra copper atom can be incorporated in the larger hole at the body center of the anti-ReO_3 structure thus forming a Cu_4N phase [5, 11].

The possibility of varying the bandgap and the metastability of Cu_3N introduces a wide variety of interesting applications in areas such as microelectronics, optical data storage, and solar energy technology. The metastability can, for example, be used for patterning of the films by various methods [12–14]. These patterns can then be used for optical data storage [15]. Another interesting large application of Cu_3N films, using the metastability, might be for metallization in microelectronics.

Films of Cu_3N are mainly produced by sputtering methods using copper and nitrogen as source materials [5–8], or by chemical processes such as chemical vapor deposition (CVD) and atomic layer deposition (ALD) where hydrogen is the most frequently used reducing agent [16, 17]. In this work the electronic structure of one Cu_3N ALD synthesized film and six differently grown CVD films have been studied together with reference samples, namely Cu_3N and $Cu(NO_3)_2$ in powder form, by means of soft x-ray absorption spectroscopy (XAS) and x-ray emission spectroscopy (XES).

2. Experimental details

2.1. Sample preparation

Films of copper(I) nitride (Cu_3N) were grown by ALD and CVD. The ALD process is described in detail by Törndahl

Table 1. Summary of the studied samples of copper(I) nitride (Cu_3N) films with deposition temperature and thickness.

Sample	Temperature (°C)
Cu_3N ALD	240
Cu_3N CVD-I	300
Cu_3N CVD-II	350
Cu_3N CVD-III	350
Cu_3N CVD-IV	360
Cu_3N CVD-V	380
Cu_3N CVD-VI	450
Cu_3N powder	—
$Cu(NO_3)_2$ powder	—

et al in [17]. The film studied here was grown using a copper(II) β-diketonate-type precursor, $Cu(hfac)_2$-hydrate [Cu(1,1,1,5,5,5-hexaflouro-2, 4-pentanedionate)$_2$] was used as the copper source material, together with deionized water and ammonia as the other precursors. The deposition temperature was 240 °C and the film thickness was 150 nm.

The studied CVD films were grown by metal organic chemical vapor deposition (MOCVD). In the MOCVD process, $Cu(hfac)_2$-hydrate, also known as copper(II) hexafluoroacetonate, was used as the copper source material together with water (deionized) and ammonia as the other precursors.

The CVD growth process consists of one step where $Cu(hfac)_2$, H_2O and NH_3 are simultaneously and continuously mixed and homogeneous reactions take place at the SiO_2 substrate. The reactants were transported into the deposition area in three separate quartz tubes in order to avoid gas mixing before reaching the substrate holder, which is made of TiN on Ti.

Of the three lines, one was designed for sublimation of the solid precursor and two lines with a constant carrier gas flow (Ar) for the supply of the gaseous precursors, water and ammonia. The deposition temperature was measured at the substrate holder with a thermocouple. The mass inlet was typically 0.7 g h^{-1} for $Cu(hfac)_2$, while the flow rate of water was varied between 0.25 and 1.8 g h^{-1} and the NH_3 flow was kept at either 5 or 20 sccm (standard cubic centimeter per minute). The experiments were carried out at in a temperature range between 300 and 450 °C, a total system pressure of 5 Torr and for a deposition time of 1 h.

The deposition temperatures of the studied samples were 300, 350, 360, 380 and 450 °C. The thicknesses of the films varied from 200 to 480 nm.

2.2. XAS, XES measurements

The soft x-ray absorption and x-ray emission measurements were performed at beamline I511-3 [18] at MaxLab in Lund, Sweden, and beamline 7.0.1 [19] at the Advanced Light Source (ALS) in Berkeley, USA. Beamline 7.0.1 employs a spherical-grating monochromator with fixed entrance slit and sliding exit slit while I511-3 is equipped with a SX-700 plane-grating monochromator.

The samples used in this study are summarized in table 1. The preparation description for each of the films can be found above. The reference samples, Cu_3N and $Cu(NO_3)_2$, were in powder form and were pressed onto small pieces of indium before being placed in the experimental chamber. Oxidation and other effects from the surfaces give small contributions to the spectra since the penetration depth of the ~400 eV photons, which were used for excitation of N Kα emission spectra, is approximately 160 nm for the studied samples [20]. All the samples were oriented with their surface plane at approximately 20° to the incident beam during the measurements.

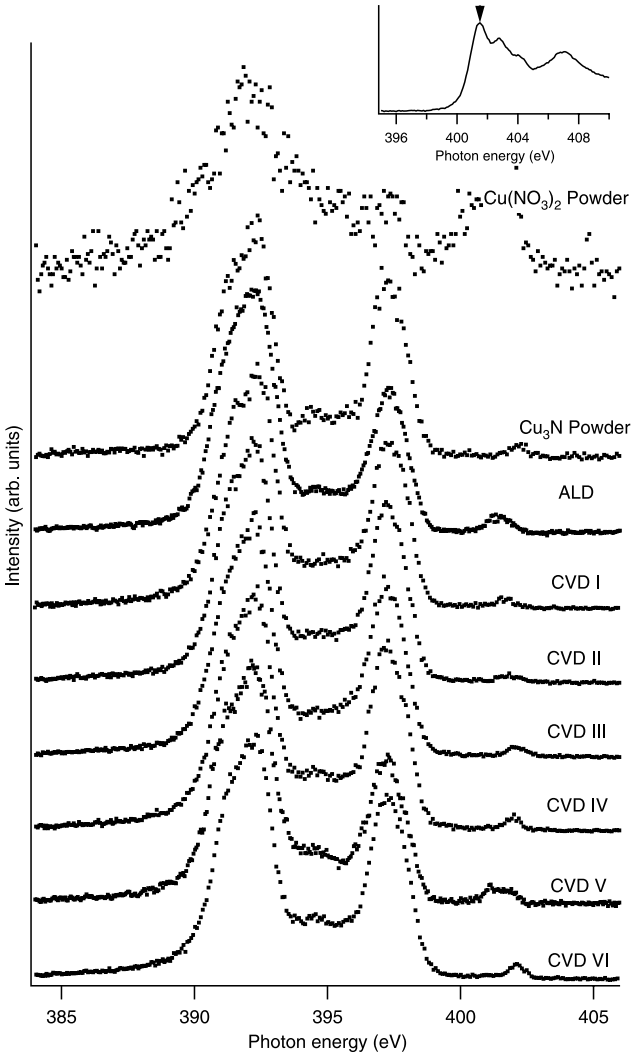

Figure 1. Resonant N Kα x-ray emission spectra for all the films and references recorded using an excitation energy tuned to the first peak of the N 1s absorption edge, as shown in the top of the panel.

The tunable x-ray emission measurements were carried out using a high-resolution grazing incidence grating spectrometer with a movable multichannel detector [21, 22]. The N Kα spectra were recorded in the first order of diffraction using a 5 m radius spherical grating with 1200 lines mm^{-1}. The experimental resolution of the monochromator was set to 1.0 eV at both MaxLab and ALS, for 400 eV and 410 eV respectively, while the spectrometer was set to a resolution of 0.2 eV, for 390 eV, at MaxLab and 0.3 eV, for 392 eV, at ALS. The N Kα emission energy scale was calibrated using overlapping reference lines from Ni inner shell transitions. The

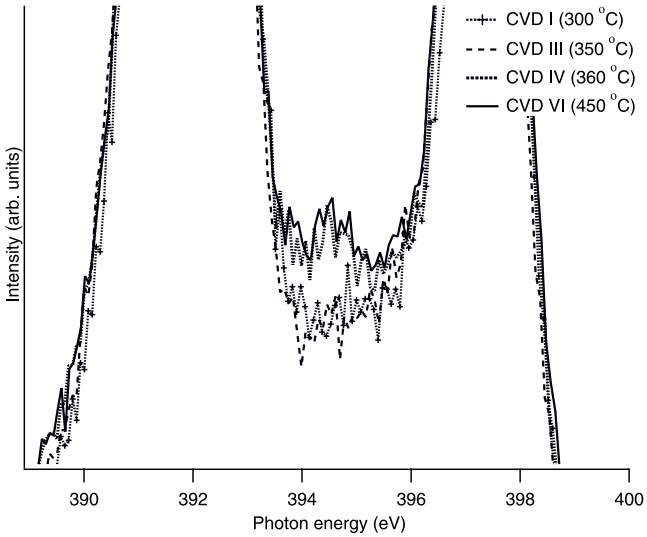

Figure 2. Closeup of the resonantly recorded spectra for CVD-I, CVD-III, CVD-IV and CVD-VI showing the temperature cut-off occurring at 360 °C.

uncertainty in calibration of the energy scales was estimated to be ±0.5 eV. To determine the excitation energies, N 1s x-ray absorption spectra were recorded in both total electron yield (TEY) and total fluorescence yield (TFY) modes.

2.3. Calculations

Calculations of the electronic structure of bulk pure Cu_3N, Cu_3N with an excess of Cu atoms, oxygen or carbon impurities, and N vacancies were done by using the projector augmented-wave method (PAW) as implemented in VASP [23] within the framework of the density functional theory (DFT). We used PAW potentials [24, 25] derived within the generalized gradient approximation (GGA) description of the electronic exchange–correlation effects [26]. 3d4p orbitals were treated as valence states for Cu and 2s2p orbitals were considered as valence states for C, N, and O atoms. A cut-off energy of 600 eV was used to ensure a convergence within 10^{-3} eV/atom of the total energy with respect to the number of plane-waves in the basis set for each studied structure at a given volume. The same degree of convergence was also achieved with respect to the number of k-points sampling of the Brillouin zone.

The electronic structure of ideal Cu_3N was calculated using the cubic anti-ReO_3-type cell (space group $Pm3m$) with copper atoms occupying the center of the cubic edges and nitrogen atoms occupying the corners of the cell. The calculated lattice parameter $a = 3.83$ and energy bandgap $E_g = 0.5$ eV are in close agreement with the results of previous calculations [27, 28]. To reach structure Cu_4N one extra copper atom was added at the center of the cubic cell. In order to calculate the change in the electronic structure due to the presence of oxygen or carbon impurities in Cu_3N we used the super-cell approximation method. We chose a super-cell made up of $2 \times 2 \times 2$ Cu_3N unit cells with a nitrogen atom being substituted by the impurity or the impurity atom being placed at the center of one of the constituent unit cells. In that case

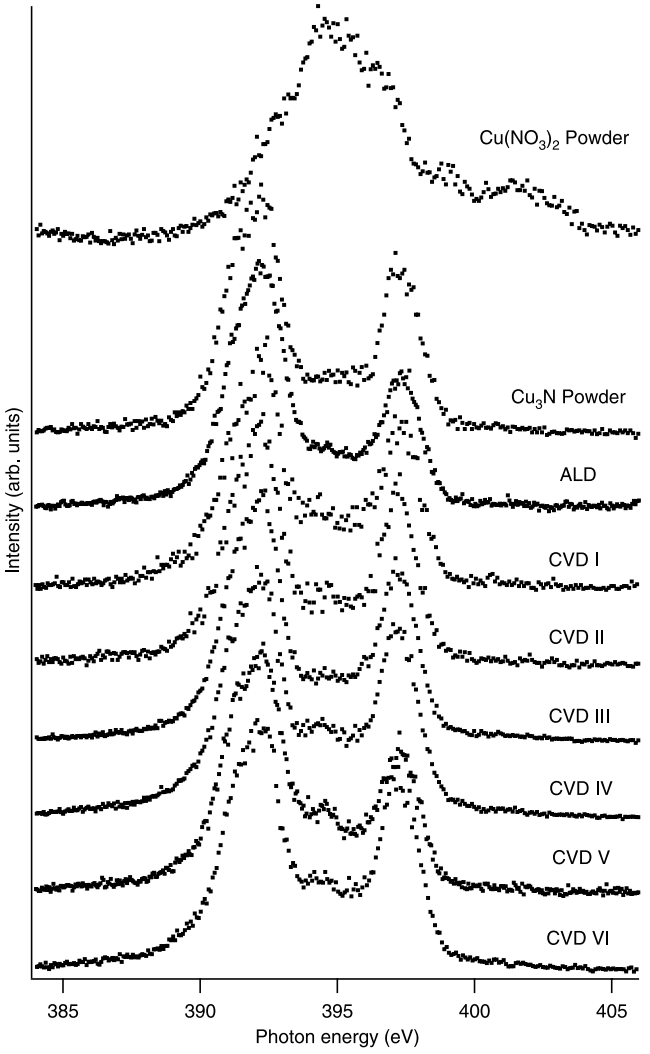

Figure 3. Non-resonant N Kα emission spectra for all films and references collected using incident photons of 430 eV.

we also performed structure optimization at fixed volume by allowing the ionic positions and the unit cell shape to relax until the Hellmann–Feynman forces acting on each ion became less than 10^{-3} eV Å^{-1}. The calculation of Cu_3N with nitrogen vacancies was performed in a similar way.

3. Results and discussion

Soft x-ray emission spectroscopy (XES) is governed by the dipole selection rules and, because the excitation is site specific, x-ray emission can be used to gain information about the local bonding environment of a sample. The nitrogen Kα spectra corresponding to 2p $\rightarrow$ 1s transitions occurs when valence band electrons with 2p symmetry fill the vacancies in the nitrogen 1s core level created by the monochromatic photon excitation. If the incident photon energy is sufficiently high, disturbances to the decay process, from the core-excited state to the final state, can occur leaving multiple vacancies in the valence band. The emission spectra recorded by tuning the incident photon energy to the N 1s threshold

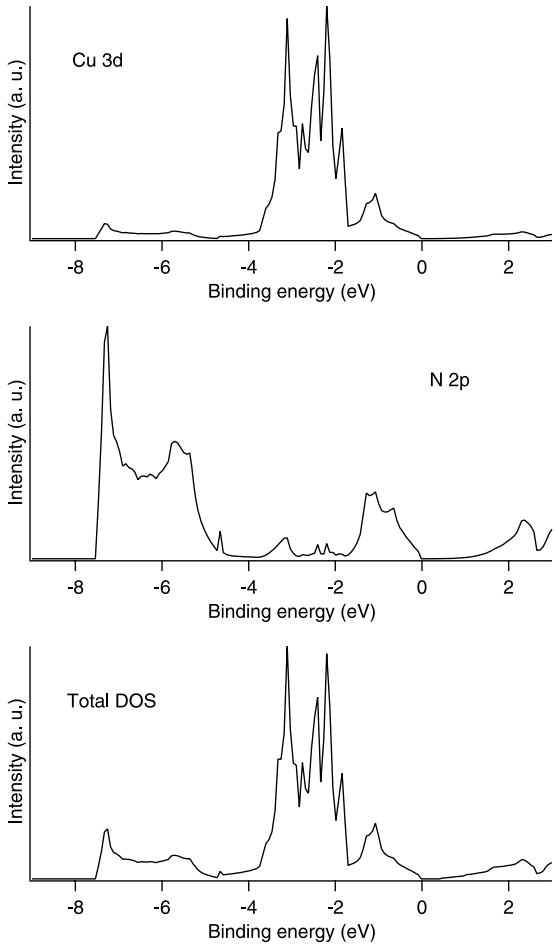

Figure 4. Partial Cu 3d DOS, partial N 2p DOS and total density of states for bulk pure Cu_3N.

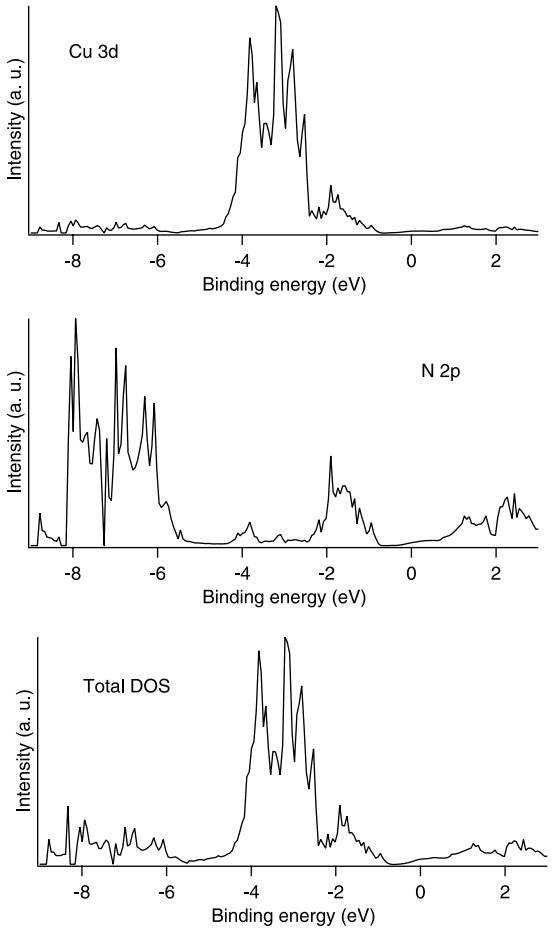

Figure 5. Partial Cu 3d DOS, N 2p DOS and total density of states for Cu_3N with oxygen impurities.

have no contribution from these multiple ionization satellites. Spectra recorded with a higher, non-resonant incident photon excitation, have a larger cross-section for multiple ionization satellites and thus the contribution from these will increase. Resonant XES with photon excitation close to the N 1s threshold therefore describes the occupied 2p states well and can be directly compared with partial density of states (DOS) calculations.

In figure 1 the measured resonant N Kα x-ray emission spectra for all the films and references are presented. All spectra were recorded using an incident photon energy tuned to the first peak in the absorption spectra for Cu_3N, i.e. the N 1s absorption peak. The excitation energy is indicated by an arrow in the inserted total electron yield spectrum at the top of the panel.

The spectra of the films are arranged in descending order according to preparation temperature, placing that of the highest temperature at the bottom. The spectra of the reference samples are shown at the top of the figure.

All studied Cu_3N films and the Cu_3N powder sample show similar main spectral shapes consisting of two dominant structures with maxima at ∼392 eV and ∼397 eV respectively. The first structure can be assigned to the main N 2p band while the second originates from Cu 3d–N 2p hybridization. There is also an additional feature present at ∼394.6 eV. This feature is more pronounced for films prepared at high temperatures while it is almost absent for low preparation temperatures. As the structure is present for CVD-IV and absent for CVD-III, figure 2, this suggests a temperature dependence with a cut-off temperature around 360 °C. The small peak at around 402 eV arises from elastically scattered incident photons.

The $Cu(NO_3)_2$ spectra shows a broader structure with a maximum at ∼391.4 eV, corresponding to the main N 2p band, with a shoulder on the high-energy side. There is also a strong peak at around 402 eV due to elastically scattered radiation.

Non-resonant N Kα emission spectra for the films and references studied are displayed in figure 3. All spectra were recorded using an excitation energy of 430.0 eV. The arrangement of the spectra is the same as for the resonant excitation spectra (figure 1).

The non-resonant spectra for the Cu_3N films and the Cu_3N powder show the same main spectral shapes as for the resonant excited spectra with two dominant intensity peaks at ∼392 and ∼397 eV corresponding to the main N 2p band and the Cu 3d–N 2p hybridization respectively. The structure at 394.6 eV is clearly present and its relative intensity appears to be slightly higher than for the resonant case. This is due to the fact that the whole region between the main 392 and 397 eV structures has a

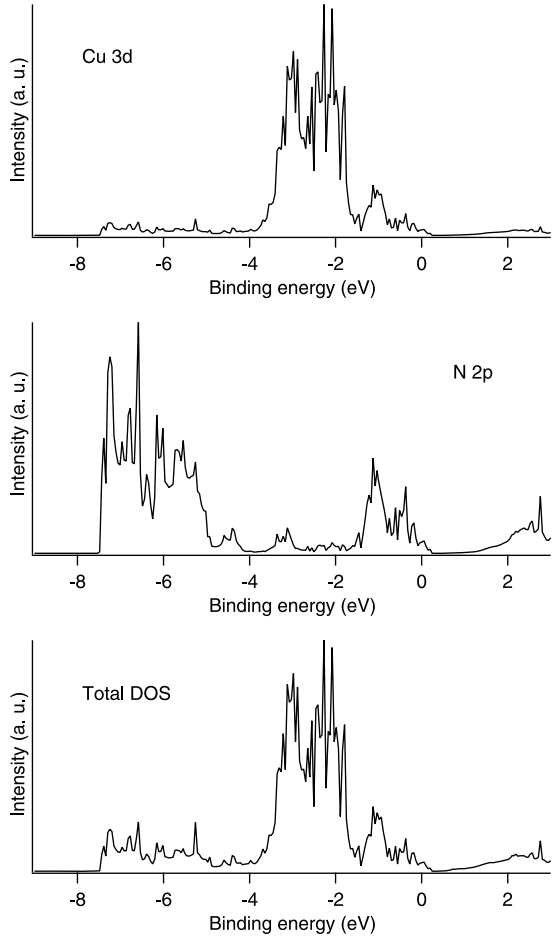

Figure 6. Partial N 2p DOS, Cu 3d DOS and total density of states for Cu_3N with carbon impurities.

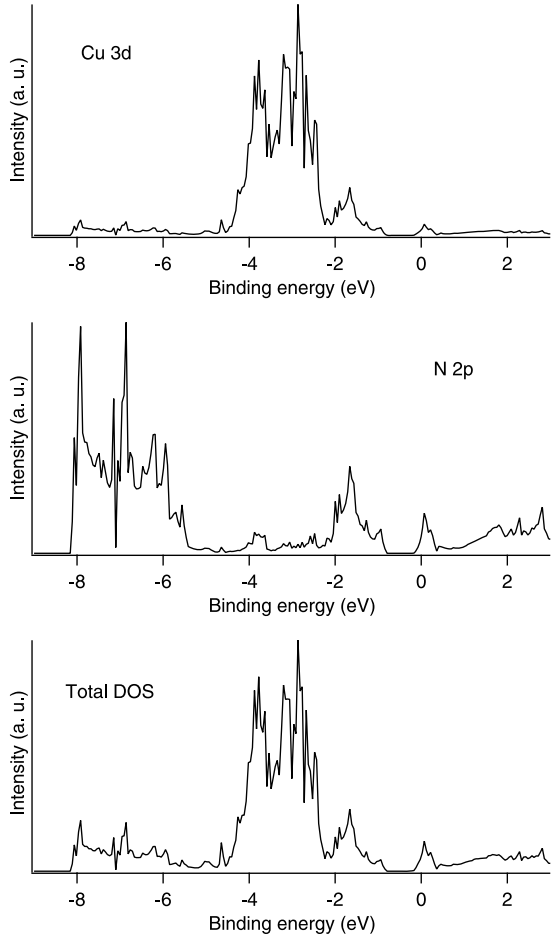

Figure 7. Partial N 2p DOS, Cu 3d DOS and total density of states for Cu_3N with nitrogen vacancies.

higher intensity than that in the resonantly excited spectra. This is most likely an effect of multiple ionization satellites, which have a higher probability of appearing at this non-resonant excitation energy.

In figures 4–8 the results of the electronic structure calculations are presented. All the figures are arranged with the partial Cu 3d DOS in the top panel, partial N 2p DOS in the middle and total density of states in the lower panel.

The electronic states of pure Cu_3N in the region of interest have a predominantly d-character (Cu 3d band), while the p states (N 2p band) contribute mostly to the energy interval close to the bottom of the valence band. These p states give rise to the first peak observed in the emission spectra, while the second observed peak is due to N p states at the top of the valence band. The calculated DOS for Cu_3N with O and C impurities and for N vacancies do not differ as much between each other and exhibit almost the same pattern as pure Cu_3N DOS, apart for the noticeable peak at the onset of the conduction band of Cu_3N with N vacancies and a less asymmetric distribution of the DOS at the bottom of the valence band, which smears out the observable features in the first emission peak. One can also see that the presence of the impurities and vacancies make the samples metallic: for O impurities and N vacancies the Fermi level lies in the conduction band, while for C impurities it lies in the valence band. As for Cu_4N, there is a very noticeable difference in both the total DOS and the partial DOS due to N p states compared to pure Cu_3N. There is a peak present at the onset at the conduction band as for Cu_3N with N vacancies, but, in addition, there is a peak in the DOS at the tail of the p states at the bottom of the valence band, which give rise to the observed structure of the main intensity peak.

Figure 9 displays all the calculated partial N 2p DOS-spectra together with the experimentally measured spectrum for the Cu_3N CVD-V film, recorded at resonant excitation. All calculated DOS-spectra are convolved with a Lorentzian, possessing a linearly energy dependent full width half maximum (FWHM), and with a Gaussian to simulate the core hole lifetime and take into account the experimental resolution.

To compare theoretical results with experimental data, the calculated spectrum based on a partial N 2p DOS for Cu_3N was placed on the emission energy scale, instead of the binding energy scale, using the recorded spectrum of the Cu_3N powder as the reference. Other calculated spectra were shifted relative to that of Cu_3N by an amount equal to the respective Fermi energy change on going from Cu_3N to the other compound. This was done to account for the relative shifts of the Fermi level in the rigid-band model and for the corresponding shifts of the core levels.

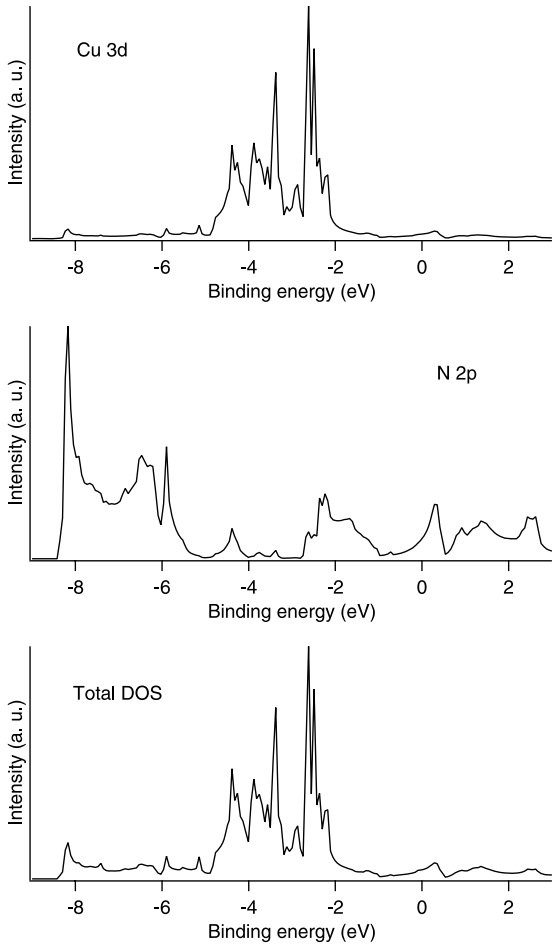

Figure 8. Partial N 2p DOS, Cu 3d DOS and total density of states for Cu_4N.

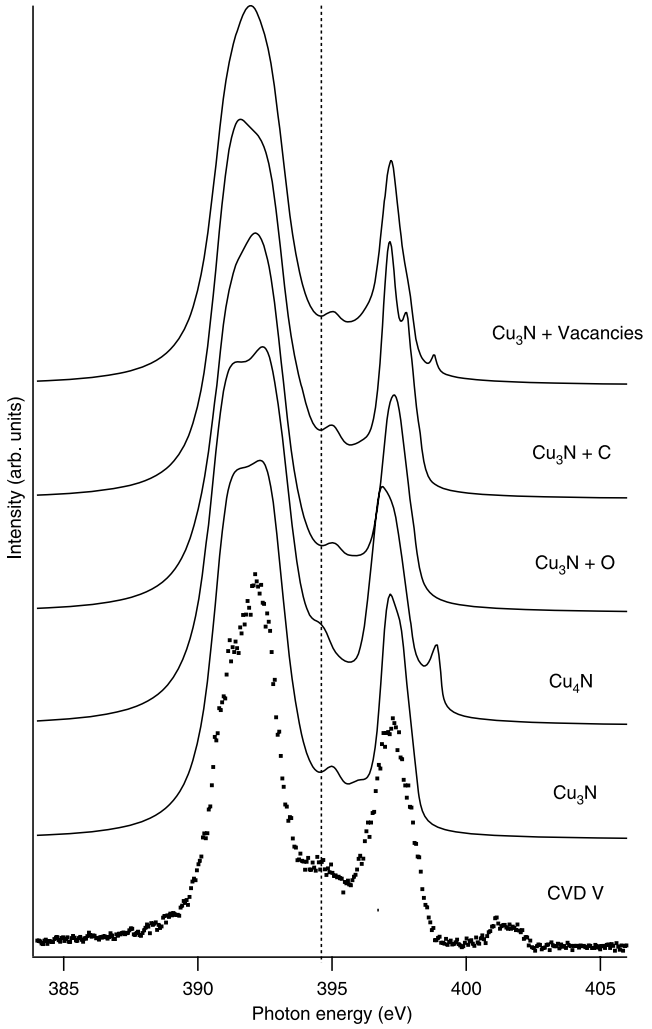

Figure 9. Partial 2p DOS of bulk pure Cu_3N, Cu_3N with an excess of Cu atoms, oxygen or carbon impurities, and N vacancies broadened to account for a variable valence 2p hole lifetime and the experimental resolution, together with resonantly excited experimental values for Cu_3N CVD-V.

All the calculated spectra show similar main spectral features as the measured spectra with the two dominant intensity peaks corresponding to the main N 2p band and the Cu 3d–N 2p hybridization. The main N 2p peak clearly consist of two features approximately 1 eV apart, for the calculated Cu_3N and Cu_4N spectra. For Cu_3N with oxygen and carbon impurities these two features are weaker, but still present, while the main peak for Cu_3N with vacancies only consists of one feature. The two features in the main N 2p band peak, are also present in the experimental spectra but the energy separation is slightly smaller, which can be partly ascribed to the somewhat narrower full width half maximum (FWHM) of the experimental spectra.

There are no great differences in the spectral shape of the peak corresponding to the Cu 3d–N 2p hybridization as the sharp features on the high-energy side in Cu_4N, Cu_3N with vacancies and Cu_3N with carbon impurities are due to the overestimated DOS contribution at the Fermi level and thus should not be present. The energy position of the peak is around 0.6 eV lower for Cu_4N than for the other compounds. This results in a smaller energy separation between the two main peaks for Cu_4N as the main N 2p peak is at the same energy position for all the studied compounds. The experimental spectra have a larger energy separation between the two main peaks than for Cu_4N but slightly smaller than for the other compounds thus suggesting that the film is a mixture of Cu_4N with some of the other compounds.

The spectral feature between the two main peaks is very similar, both in energy position and appearance, for bulk pure copper nitride, Cu_3N with carbon and oxygen impurities, and for Cu_3N with vacancies. For Cu_4N this feature is closer to the main N 2p band peak and much higher in intensity. This spectral feature lies within the region of 12 non-bonding bands which separates 3 Cu 3d–N 2p bonding bands (lower energy region) and 3 Cu 3d–N 2p anti-bonding states (energy region below the Fermi level). The orbital character of the non-bonding states is mainly d (Cu 3d), but within the region of the main N 2p peak a few bands have a smaller degree of p orbital character. These N 2p states seem to be hybridized mainly with Cu 3d states, while, within the bonding and anti-bonding region, the hybridization with Cu 4s and Cu 4p states also plays an important role in the formation of covalent bonds. When the experimental spectra also has this peak closer to the main

peak, this, together with the fact that the peak is more likely to gain intensity around this energy, suggests that the major contribution of this feature in the studied films originates from Cu_4N species.

From the discussion above it can be concluded that the electronic structure calculations are in good agreement with the experimentally recorded spectra for the studied films. The calculation results support the proposed theory that films prepared in copper rich environments and above the cut-off temperature of 360 °C have a growing fraction of areas with an excess of copper, while films prepared below this temperature do not have these copper enriched areas. That this was not seen in the preliminary x-ray diffraction (XRD) measurements on the studied films can be explained by the fact that these measurements probe the long range order of the structure of the films and therefore will not see small fractions of copper enriched regions. Soft x-ray emission spectroscopy, on the other hand, is a local probe and can therefore also detect very small fractions of different copper content as long as they give rise to intensities at specific energies.

4. Conclusions

By using tunable soft x-ray emission spectroscopy, supported by electronic structure calculations, it could be concluded that the studied copper nitride films grown with chemical vapor deposition in copper rich environments and above 360 °C had an increased fraction of copper enriched areas. These localized areas with a slightly different copper content could be seen with soft x-ray emission spectroscopy, as this method is a local probe. The excess copper in these areas gave rise to an increase in intensity between the two main peaks in the nitrogen Kα spectra.

Acknowledgments

We are grateful to the personnel at beamline I511-3, MaxLab and beamline 7.0.1 at the Advanced Light Source for their assistance during the XES and XAS measurements.

The Advanced Light Source is supported by the Director, Office of Science, Office of Basic Energy Sciences, of the US Department of Energy under Contract No. DE-AC02-05CH11231.

References

[1] Braun K F 1874 *Ann. Phys. Chem.* **153** 556
[2] Bardeen J and Brattain W H 1948 *Phys. Rev.* **74** 230
[3] Shockley W 1949 *Bell Syst. Tech. J.* **28** 435
[4] Pierson J F 2002 *Vacuum* **66** 59
[5] Maruyama T and Morishita T 1995 *J. Appl. Phys.* **78** 4104
[6] Nosaka T, Yoshitake M, Okamoto A, Ogawa S and Nakayama Y 1999 *Thin Solid Films* **348** 8
[7] Kim K J, Kim J H and Kang J H 2001 *J. Cryst. Growth* **222** 767
[8] Ghosh S, Singh F, Choudhary D, Avasthi D K, Ganesan V, Shah P and Gupta A 2001 *Surf. Coat. Technol.* **142–144** 1034
[9] Soukup L *et al* 1999 *Surf. Coat. Technol.* **116–119** 321
[10] Borsa D M and Boerma D O 2004 *Surf. Sci.* **548** 95
[11] Blucher J, Bang K and Giessen B C 1989 *Mater. Sci. Eng.* A **117** L1
[12] Asano M, Umeda K and Tasaki A 1990 *Japan. J. Appl. Phys.* **29** 1985
[13] Nosaka T, Yoshitake M, Okamoto A, Ogawa S and Nakayama Y 2001 *Appl. Surf. Sci.* **169/170** 358
[14] Maya L 1993 *Mater. Res. Soc. Symp. Proc.* **282** 203
[15] Cremer R, Witthaut M, Neuschutz D, Trappe C, Laurenzis M, Winkler O and Kurz H 2000 *Mikrochim. Acta* **133** 299
[16] Pinkas J, Huffman J C, Baxter D V, Chisholm M H and Caulton K G 1995 *Chem. Mater.* **7** 1589
[17] Törndahl T, Ottosson M and Carlsson J-O 2006 *J. Electrochem. Soc.* **153** C146
[18] Denecke R, Vaterlein P, Bassler M, Wassdahl N, Butorin S, Nilsson A, Rubensson J-E, Nordgren J, Martensson N and Nyholm R 1999 *J. Electron Spectrosc. Relat. Phenom.* **101–103** 971
[19] Warwick T, Heimann P, Mossessian D, McKinney W and Padmore H 1995 *Rev. Sci. Instrum.* **66** 2037
[20] http://henke.lbl.gov/optical_constants/filter2.html
[21] Nordgren J and Nyholm R 1986 *Nucl. Instrum. Methods Phys. Res.* A **246** 242
[22] Nordgren J, Bray G, Cramm S, Nyholm R, Rubensson J-E and Wassdahl N 1989 *Rev. Sci. Instrum.* **60** 1690
[23] Kresse G and Furthmüller J 1996 *Phys. Rev.* B **54** 11169
[24] Blöchl P E 1994 *Phys. Rev.* B **50** 17953
[25] Kresse G and Joubert D 1999 *Phys. Rev.* B **59** 1758
[26] Perdew J P, Chevary J A, Vosko S H, Jackson K A, Pederson M R, Singh D J and Fiolhais C 1992 *Phys. Rev.* B **46** 6671
[27] Hahn U and Weber W 1996 *Phys. Rev.* B **53** 12684
[28] Moreno-Armenta M G, Martinez-Ruiz A and Takeuchi N 2004 *Solid State Sci.* **6** 9